RSC Mechanochemistry

ROYAL SOCIETY OF CHEMISTRY

PAPER

View Article Online
View Journal

Cite this: DOI: 10.1039/d5mr00122f

Sono-mechanical activation-assisted proton-catalyzed self-polymerization of AMPS in water: hydrogel formation and its application as a functional additive in ordinary Portland cement

Kuldeep Rajpurohit, Sabrina A. Shaikh, Ashok K. Pandey * and Hemlata K. Bagla*

A green, initiator-free method for polymerizing 2-acrylamido-2-methyl-1-propane sulfonic acid (AMPS) was developed using low-frequency ultrasound (20 ± 3 kHz) in aqueous solution. Unlike conventional sonochemistry, where radical formation occurs *via* water sonolysis, the radical generation originates directly from the AMPS monomer, as verified by ESR, DPPH radical scavenging assays and NMR experiments. ESR experiments indicated the radical formation on AMPS at elevated temperatures, which was lowered by cavitation-induced shear forces caused by low-frequency ultrasound. Water functions as a medium for proton-assisted activation, as no polymerization occurs in aprotic solvents, such as DMF and 1-decanol, as well as a hydrogen-bonded deep eutectic solvent (choline chloride : ethylene glycol in a 1 : 2 mol proportion). Comparative experiments showed that acrylamide, methacrylic acid, and (3-acrylamidopropyl)trimethylammonium chloride failed to polymerize ultrasonically, underscoring the unique reactivity of AMPS. AMPS also polymerized under microwave heating, albeit at a higher temperature, further confirming that cavitation-induced mechanical activation assists but does not solely govern radical formation. Mechanistic validation was obtained through model reactions involving acrylamide polymerization in the presence of methane sulfonic acid (1 : 1 mol ratio), and AMPS did not polymerize in its neutralized Na^+ form. These results establish that the sulfonic acid group serves dual functions, as a proton donor and as a charge-balancing counterion, thereby enabling an acid-assisted, hydrogen-bond-directed radical polymerization pathway under sono-mechanical activation. The poly(AMPS) hydrogels were characterized by FESEM, thermal analysis and swelling experiments. The tunable swelling behavior, governed by the crosslinker density, was observed with water uptake decreasing from 1678 wt% at 2 mol% MBA to 250 wt% at 15 mol%. Lightly crosslinked gels exhibited self-healing behavior driven by reversible hydrogen bonding. GPC and viscosity analyses revealed simultaneous cavitation-induced depolymerization and radical polymerization, similar to ionizing radiation-based polymerization, though rapid crosslinking stabilized the hydrogel network. The incorporation of functional polymeric hydrogels into cementitious systems has emerged as an effective strategy for modifying hydration behavior, mechanical performance, and microstructural development. The cross-linked poly(AMPS) hydrogel was used in its calcium form (Ca-poly(AMPS)) as an additive in ordinary Portland cement, and its effect was evaluated as functions of setting time, compressive strength, tensile strength, and heat of hydration.

Received 4th October 2025
Accepted 16th March 2026

DOI: 10.1039/d5mr00122f

rsc.li/RSCMechanochem

1. Introduction

Hydrogels are soft materials that find extensive applications in wastewater treatment,[1,2] energy storage,[3,4] agriculture,[5,6] tissue engineering,[7] food science,[8] sensor development,[9] self-healing cement,[10] flexible electronics,[11] and separation science.[12,13] Hydrogels have three-dimensional polymer networks that absorb large amounts of water, providing active sites for adsorption. The stability of hydrogels under stress is achieved through chemical or physical crosslinking, hydrogen bonding, or interpenetrating networks. Synthetic hydrogels, typically prepared by the free radical polymerization of hydrophilic acrylate monomers, are preferred over biopolymer hydrogels due to their tuneable properties.[14] Free radical polymerization can be initiated by heat, light, or ionizing radiation, with thermal initiation being most common in industry.[15] Large-scale production requires scalability, safety, and purity, especially for biomedical uses. Water-soluble acrylate monomers

Department of Nuclear and Radiochemistry, Kishinchand Chellaram College, HSNC University, Mumbai-400020, India. E-mail: ashok.pandey@kccollege.edu.in; hemlata.bagla@kccollege.edu.in

and crosslinkers are favoured, as they allow easy removal of residual chemicals and avoid harmful solvents. Ionizing radiation-based free radical polymerization offers the added benefit of simultaneous sterilisation.[16] However, its wider use is limited by cost and availability.

Mechanochemical activation-based free radical polymerization offers several advantages, such as solvent-free polymerization, the possibility of new synthetic chemistry, no dependency on the solubility of monomer and precipitation, and controlled polymerization.[17] The mechanochemical activation of polymerization or depolymerization is based on the utilization of mechanical forces generated by ball-milling to generate reactive free radicals. Ball milling and grinding provide higher shear forces that lead to solid-state polymerization of many vinyl monomers without the need for initiators.[17] Another type of mechanochemical polymerization is activation by ultrasonication at high frequencies, which is well-suited for solvent media.[18,19] The use of ultrasonic activation for chemical reactions is known as sonochemistry.[20] Suslick classified mechanochemistry into four categories depending upon the manner of applying mechanical force, *i.e.* tribochemistry (the chemistry of surfaces in contact), trituration (chemistry induced by grinding and milling), macromolecular mechanochemistry (from breakage of polymer chains to molecular motors and biological motion), and sonochemistry (the chemistry generated from the mechanical consequences of sound).[21] Ultrasonic waves in liquid media generate heat, shock waves, and microstreaming *via* cavitation, enhancing molecular motion.[22] The sonochemical reactions could be attributed to mechanical forces generated due to shock waves and molecular motions, and free radicals formed due to cavitation, which can be varied by the frequency and intensity (power) of applied ultrasonication.[23]

Sonochemical radical generation increases with frequency up to a maximum in the mid-to-high range (~300–800 kHz), after which it declines.[23] At low frequencies, cavitation bubbles collapse violently due to their larger radius, producing strong shear forces but relatively lower radical yields. In contrast, ~500 kHz offers optimal radical formation, whereas at ~1 MHz, the bubble size is too small for effective collapse, leading to negligible radical production.[24] The cavitation is a major factor for mechanochemical activation by ultrasound.[25] Free radical polymerization at low frequencies (20–40 kHz) requires high power input and controlled conditions, including an inert atmosphere, increased viscosity (*e.g.*, with glycerol), emulsion polymerization using sodium dodecyl sulfate, *etc.*[26–29] At ~500 kHz, polymerization proceeds more efficiently due to enhanced radical availability.[30] Alternatively, chemical initiators such as AIBN, BPO, or sodium persulfate readily decompose under low-frequency cavitation (~20 kHz) and have been extensively applied in bulk gel synthesis and *in situ* gel formation within porous polymer membranes.[31–33]

The additive-free sono-mechanical polymerization is the sustainable green route for the bulk production of high-purity hydrogels for commercial-scale applications such as healthcare or polymer-reinforced green cement. Therefore, this study intended to develop a sustainable, additive-free water-based method for synthesizing poly(2-acrylamido-2-methyl-1-propane sulfonic acid) (poly-AMPS)-based hydrogels through sono-mechanical-activation at a low frequency (20 ± 3 kHz) of ultrasound, focusing on understanding the mechanism of polymerization, characterization of properties of hydrogel and tuning properties for the desired applications. The cross-linked poly(AMPS) hydrogel in its calcium form (Ca-poly(AMPS)) has been studied as a functional additive in ordinary Portland cement for understanding its effects on hydration kinetics, setting time, compressive strength, and tensile strength in the cementitious materials.

2. Experimental

2.1. Materials & instruments

Analytical reagent-grade chemicals and de-ionized water were used in the experiments. 2-Acrylamido-2-methyl-1-propane sulfonic acid (AMPS), acrylamide, *N*,*N*′-methylene-bis-acrylamide (MBA) and 2,2-diphenyl-1-picrylhydrazyl (DPPH) were procured from Sigma-Aldrich (Steinem, Switzerland). *N*,*N*′-Dimethyl formamide (DMF) was obtained from S.D. Fine Chem. Ltd, Mumbai, India. The functional groups of the hydrogel and monomer were analyzed using a PerkinElmer FTIR spectrometer equipped with an ATR module. The spectra were recorded with a resolution of 4 cm^{-1} over a range of 400 to 4000 cm^{-1}, utilizing 16 scans for each measurement. An Ostwald viscometer was used for measuring the viscosity of a solution containing uncrosslinked poly(AMPS). Surface and elemental composition analyses of the hydrogel were conducted by Field Emission Scanning Electron Microscopy (FESEM) (JEOL JSM-7600F) with Energy Dispersive X-ray Spectroscopy (EDS) mapping. The hydrogel samples for FESEM with EDS mapping were coated with a 10 nm layer of platinum to prevent charging effects. Micrographs were captured at magnifications ranging from 300× to 30 000× and at an accelerating voltage of 20 kV. Gel permeation chromatography (GPC) analysis of uncrosslinked poly(AMPS) in water was carried out using an 1260 Infinity II GPC system. An ultrasonic probe sonicator (model DP 700, procured from Gravity Laboratory) with 20 ± 3 kHz frequency, 700 watts power, and a 1.5 cm titanium probe was used to prepare hydrogels. Electron spin resonance (ESR) spectroscopy was performed on a JEOL JES-FA200 spectrometer (X-band: 8.75–9.65 GHz; sensitivity: 7 × 10^9 spins/0.1 mT; resolution: 2.35 μT) equipped with aqueous, electrochemical, UV-irradiation, sample-mixing, and angular-rotation accessories. Thermogravimetric analysis (TGA) was conducted using a Hitachi NEXTA STA-300 (RT to 1500 °C; operating up to 1300 °C; heating rate: 0.1–100 °C min^{-1}). Differential scanning calorimetry (DSC) was carried out on a Hitachi DSC7020 (−150 °C to 725 °C; 0.1–100 °C min^{-1}) under N_2 flow (50–500 mL min^{-1}) with liquid-nitrogen cooling. Nuclear magnetic resonance (NMR) spectra were recorded in D_2O on a JEOL ECZR 600 MHz spectrometer fitted with a 5 mm multinuclear broadband probe and a TH5 variable-temperature probe (−100 °C to +150 °C) with automatic tuning and matching.

2.2. Preparation of poly(AMPS) hydrogels

Poly(AMPS) and crosslinked poly(AMPS) hydrogels were synthesized using 2-acrylamido-2-methyl-1-propane sulfonic acid (AMPS) as the monomer and AMPS with *N*,*N*′-methylene-bis-acrylamide (MBA) as the crosslinker, respectively. The choice of this monomer and crosslinker was based on the fact that both are acrylate-based and have hydrogen bonding groups. The hydrogels were prepared by taking desired amounts of AMPS and 10 mol% of MBA in 20 mL of deionized water. This solution was sonicated with an ultrasonic probe sonicator from 5 to 20 min using 148 W cm^{-2} power. For making uncrosslinked poly(AMPS), the polymerizing solution was sonicated under identical conditions without the crosslinker MBA. Similar experiments were carried out using AMPS with varying molar proportions of MBA in deionized water to achieve different degrees of crosslinking following a similar protocol.

2.3. Characterization studies

The equilibrium swelling of the hydrogels was determined by immersing dried samples in a neutral pH medium (pH 6.5–7.5) at room temperature. After 24 h, the samples were removed, gently blotted with paper to eliminate excess surface water, and weighed. The hydrogels were further soaked to verify consistent swelling for 8 h, with weight measurements taken every hour. The equilibrium swelling was calculated as water uptake (%) using the following equation:

$$\text{Water uptake}(\%) = \frac{W_t - W_0}{W_0} \times 100$$

where W_0 represents the dried gel weight and W_t is the gel weight after swelling in water. Each swelling experiment was performed in triplicate to ensure accuracy and reproducibility. Similar experiments were carried out to study the pH responsiveness of the hydrogel by equilibrating 1 g of hydrogel samples in solutions having pH values of 1, 7, and 13. To examine the influence of ionic strength, a separate experiment was conducted where the hydrogel was equilibrated in a 0.5 M NaCl solution.

The formation of free radicals was studied by the radical scavenging assay using DPPH as described elsewhere.[34] To prepare the DPPH solution for the radical scavenging assay (RSA), 0.08 mg of DPPH was dissolved in 100 mL of methanol to achieve a 0.2 μM concentration. In the RSA assay, several sample combinations were prepared to study the radicals scavenging by DPPH during polymerization. The test sample included two conditions: one containing 5 g of AMPS, 0.39 g of MBA, and 10 mL of distilled water combined with 10 mL of DPPH solution and another prepared without the DPPH solution, using only 5 g of AMPS, 0.39 g of MBA, and 10 mL of distilled water. To establish baseline controls, a negative control was prepared by mixing 10 mL of DPPH solution with 10 mL of distilled water, while a positive control consisted of 5 g of AMPS combined with 10 mL of DPPH solution. Each mixture was allowed to react for 5 minutes, providing sufficient time for interaction between free radicals and DPPH, thus enabling accurate RSA measurements under different conditions. The absorbance at 517 nm was monitored using a UV-visible spectrophotometer. The RSA percentage was calculated using the following formula:[35]

$$\text{RSA} = \frac{(B - T)}{B} \times 100$$

where B represents the absorbance of the control sample and T is the absorbance of the test specimen.

To investigate the effect of sonication on the viscosity of poly(AMPS) solutions, a series of experiments were conducted with varying poly(AMPS) concentrations and sonication times. Each experiment measured the changes in viscosity using an Ostwald viscometer at specific time intervals, providing insight into how sonication influences the rheological behaviour of AMPS solutions. The molecular weight determination of uncrosslinked poly(AMPS) was carried out by GPC using water as a solvent and PEG/PEO as the standards for calibration.

2.4. Application in ordinary Portland cement

OPC 53 grade ordinary Portland cement (OPC) was used with standard quartz sand conforming to BIS specifications (IS 650:1966), consisting of three equal fractions: Grade I (1–2 mm), Grade II (500 μm–1 mm), and Grade III (90–500 μm). The setting time was determined using a Vicat apparatus as per IS 5513:1976. Mechanical properties were evaluated by measuring tensile strength (IS 269:1958) and compressive strength using a 2000 kN capacity motorized hydraulic compression testing machine. The heat of hydration was measured using a calorimeter as per the Bureau of Indian Standards (BIS) protocol.[36] The exact compositions of the samples are given in the Experimental section (SI) and described briefly below.

Poly(AMPS) hydrogels crosslinked with 5, 10, and 15 mol% of MBA were immersed in 0.1 M $CaCl_2$ solution to convert these into Ca^{2+} forms. The Ca^{2+}-equilibrated gels were dried before mixing with OPC. The Ca^{2+}-equilibrated hydrogel was added in varying amounts, 0 (control), 0.3, 0.5, 1.0, and 2.0 wt%, to a mix of 398 ± 2 g of OPC with 102 g of distilled water. The water content corresponded to 0.85 times water required for normal consistency (30 wt% of OPC weight). Mixing was completed within 3–5 min at 27 ± 2 °C and 65 ± 5% relative humidity. The initial and final setting times were determined using a Vicat apparatus in accordance with BIS.[37]

Mortar for the control mix was prepared using 200 g of cement, 600 g of standard sand, and 84 g of distilled water. In hydrogel-modified mortars, OPC was replaced with 0.3, 0.5, 1.0, and 2.0 wt% hydrogel, corresponding to 199.4 g cement + 0.6 g gel, 199.0 g cement + 1.0 g gel, 198.0 g cement + 2.0 g gel, and 196.0 g cement + 4.0 g gel, respectively, while keeping the sand (600 g) and water content (84 g) constant. The mortar was placed in 70.6 mm cube moulds in three layers, each layer being tamped and subsequently compacted on a vibrating table at 12 000 ± 400 vibrations per min for 2 min. After 24 h of moist curing at 27 ± 2 °C and ≥90% RH, the specimens were demoulded and cured in water for 7, 28, and 60 days. The compressive strength was obtained as the average of three specimens as per the BIS method.[38]

For tensile strength determination, the control mortar consisted of 40 g of cement, 120 g of standard sand, and 16.8 g of distilled water. Hydrogel-modified mixes were prepared by replacing OPC partially with 0.12, 0.20, 0.40, and 0.80 g of hydrogel, while maintaining constant sand and water contents. The mortar was cast in briquette moulds in three layers with proper tamping and vibration, stored under moist conditions for 24 h, demoulded, and water-cured for 7, 28, and 60 days. Tensile strength was determined in triplicate in accordance with the BIS protocol.[39]

For the calorimetric study, the control paste consisted of 60 g of cement and 24 g of distilled water. In hydrogel-modified systems, OPC was replaced partially with 0.18, 0.30, 0.60, and 1.20 g of hydrogel, while maintaining a constant water content of 24 g. The paste was hand-mixed for 4 min, transferred to sealed plastic containers, and stored in a vertical position until testing at 7, 28, and 60 days. The heat capacity of the calorimeter was determined using a standard ZnO reaction in a solution containing 2 N HNO_3 and HF. The heat of solution of anhydrous cement and hydrated cement was measured by recording the temperature rise after dissolution in the acid mixture. The heat of hydration was calculated from the difference between the heat of solution of anhydrous and hydrated cement in accordance with BIS.[35]

3. Results and discussion

3.1. Formation of the hydrogel

The crosslinked poly(AMPS) hydrogel was readily formed in water using 20 kHz ultrasound at a power density of 148 W cm^{-2}. Higher power was avoided to limit heat build-up. However, the solution temperature increased to ≈60 °C after 5 min of sonication and to ≈70 °C after 20 min. It was observed that the simple thermal heating at 70 °C for 30 min did not produce a hydrogel, confirming that gelation is not thermally driven. The choice of 20 kHz ultrasound was based on its well-established ability to produce intense cavitation. In this frequency range, shear forces generated from cavity collapse are maximal, whereas radical formation from water sonolysis is minimal.[23,24] Consistent with this, radical scavenging assays using DPPH, performed under identical power and duration used for polymerization, showed no detectable radical generation in DI water. It was also observed that gelation also occurred under microwave irradiation, a condition that does not generate cavitation-derived radicals, indicating that the polymerization does not rely on radicals produced from water sonolysis. Collectively, these results support that polymerization at 20 kHz is driven predominantly by sono-mechanical activation of the AMPS monomer *via* shear forces induced by cavitation.

To clarify how the monomer structure governs sono-mechanical polymerization, a series of acrylate-based monomers with distinct functional groups were examined under identical 20 kHz sonication conditions using 10 mol% MBA as the crosslinker. The chemical structures of monomers are shown in Fig. 1. Monomers representing weakly acidic (methacrylic acid), neutral (acrylamide), and strongly basic ((3-acrylamidopropyl)trimethylammonium chloride, APMAC)

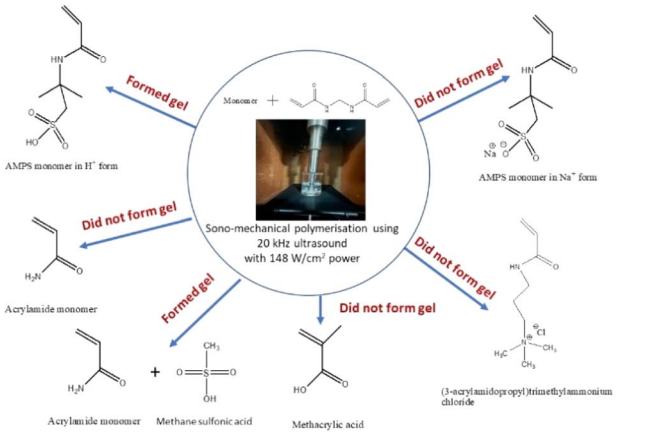

Fig. 1 Chemical structures of monomers used for sono-mechanical polymerization with MBA as the crosslinker, illustrating that crosslinked gel formation occurs only under acidic conditions (presence of H^+ ions).

functionalities, as well as AMPS in both its protonated (H^+) and sodium (Na^+) forms, were evaluated. Under prolonged sonication, none of the compared monomers underwent polymerization to form crosslinked hydrogels of poly(APMAC), poly(methacrylic acid), or poly(acrylamide), suggesting that neither neutral nor weakly acidic or strongly basic functionalities support sono-mechanical polymerization. Although methacrylic acid contains an acidic group, its acidity is far lower than that of sulfonic acid present in AMPS. Importantly, AMPS differs from APMAC only in the functional groups. AMPS carries a sulfonic acid moiety, whereas APMAC bears a quaternary ammonium cation. As shown in Fig. 1, AMPS contains both an amide segment (similar to acrylamide) and an alkane sulfonic acid unit, strongly suggesting that the sulfonic acid group plays an important role in enabling sono-mechanical polymerization. To verify this, acrylamide was polymerized in the presence of methane sulfonic acid (1 : 1 molar ratio). Under the same sonication conditions used for AMPS, a crosslinked poly(acrylamide) gel formed readily. Acrylamide also formed a gel in 0.01 M H_2SO_4. These experiments, summarized in Table S1 (SI), consistently demonstrated that sulfonic acid groups promoted polymerization under sono-mechanical activation.

The effect of solvent and monomer concentration on the sono-mechanical formation of poly(AMPS) gels (10 mol% MBA) showed that gelation occurred exclusively in water, while no gel formed in DMF, 1-decanol and the deep eutectic solvent (DES) formed from choline chloride and ethylene glycol in a 1 : 2 mol proportion, having low viscosity. This solvent dependence is consistent with the unique cavitation properties of water, its high vapor pressure, low viscosity, and high surface tension, which promote efficient bubble formation and collapse, enabling effective mechanical activation of AMPS. Water also dissolves AMPS uniformly due to its strong polarity and hydrogen-bonding ability, preventing phase separation that can occur in DMF or 1-decanol, where polarity mismatch limits AMPS solubility. As reported in the literature, phase-transfer catalysts can sometimes overcome such incompatibility,[27,28]

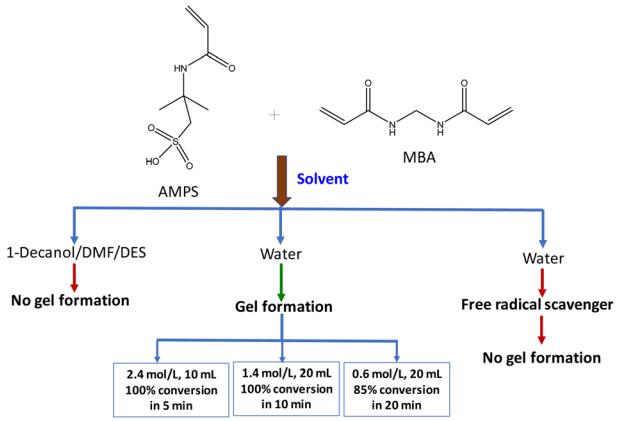

Fig. 2 Formation of the MBA crosslinked poly(AMPS) gel in different solvents, with varying conc. of AMPS.

but without them polymerization is inefficient in these nonaqueous media. Additionally, the hydrogen-bonding environment of water stabilizes short-lived reactive intermediates, and its high thermal conductivity helps dissipate heat generated during cavitation, minimizing undesirable side reactions. In contrast, differences in physicochemical properties of DMF and 1-decanol, including vapor pressure and surface tension, alter the cavitation bubble dynamics and reduce the efficiency of energy transfer. Despite its moderate viscosity (~40 cP), the crosslinked poly(AMPS) gel could not be formed due to reduced AMPS ionization, which prevented H^+ ion catalyzation for the formation of free radicals on AMPS.

The requirement for proton availability was further validated by converting AMPS into its Na^+ form, see Fig. 1. When the monomer solution was neutralized with NaOH (pH ≈ 7) and subjected to identical sonication conditions, AMPS–Na^+ failed to form a hydrogel despite the presence of MBA. This clearly shows that protonated AMPS is necessary for chain activation and propagation and that neutralization effectively suppresses polymerization.

While these solvent properties influence cavitation, it can be seen from Fig. 2 that cavitation primarily serves to provide the activation energy needed for proton-assisted initiation of AMPS. Once this activation occurs, the subsequent polymerization becomes strongly dependent on the monomer concentration rather than on bulk solvent characteristics. This trend is evident in Fig. 2, *i.e.* increasing AMPS concentration accelerates gelation and increases conversion. For example, 2.4 mol L^{-1} results in complete gelation in 5 min, while 0.6 mol L^{-1} results in only 85% conversion in 20 min. Although increasing the water volume from 10 mL to 20 mL changes the total liquid volume, it dilutes the monomer and lowers the local concentration of reactive species, an effect that directly slows network formation. Consequently, gelation time is only weakly sensitive to moderate changes in total solvent volume, because the rate-determining steps, after sono-mechanical activation, are governed by monomer availability and spatial proximity rather than by differences in cavitation intensity across these volumes. It was also observed that gelation time was affected by sonication power, and no gelation was observed below a threshold, which was 50 W cm^{-2} in the present case. It was observed that the poly(AMPS) hydrogel was not obtained in the presence of the free-radical scavenger DPPH, confirming that polymerization occurred through a free-radical polymerization mechanism.

3.2. Heating effects on AMPS

To distinguish the effect of simple thermal treatment from that of sono-mechanical activation, ^{1}H NMR and ESR measurements were carried out at elevated temperatures and compared with those performed at room temperature. The ^{1}H NMR spectrum of AMPS in D_2O at room temperature shown in Fig. 3a exhibits sharp and well-resolved resonance characteristics of the monomeric form (δ 6.10 (dd, J = 17.1, 10.3 Hz, 1H), 6.04–5.96 (m, 1H), 5.60–5.53 (m, 1H), 3.29 (s, 2H), 1.38 (s, 6H)). The ^{1}H NMR spectrum shows well-resolved vinyl proton signals between 6.1 and 5.5 ppm with characteristic coupling patterns as can be seen from zoomed spectrum given in inset of Fig. 3a, indicating the freely dissolved monomer. As can be seen from Fig. 3b, the spectrum exhibited marked differences in the ^{1}H NMR spectrum of AMPS at 80 °C (δ 6.80–6.36 (m, 2H), 6.17–6.01 (m, 1H), 3.92–3.59 (m, 2H), and 2.13–1.70 (m, 6H)). The signals broaden and partially merge into multiplets in the 6.80–6.01 ppm region. The persistence of the vinyl proton signals

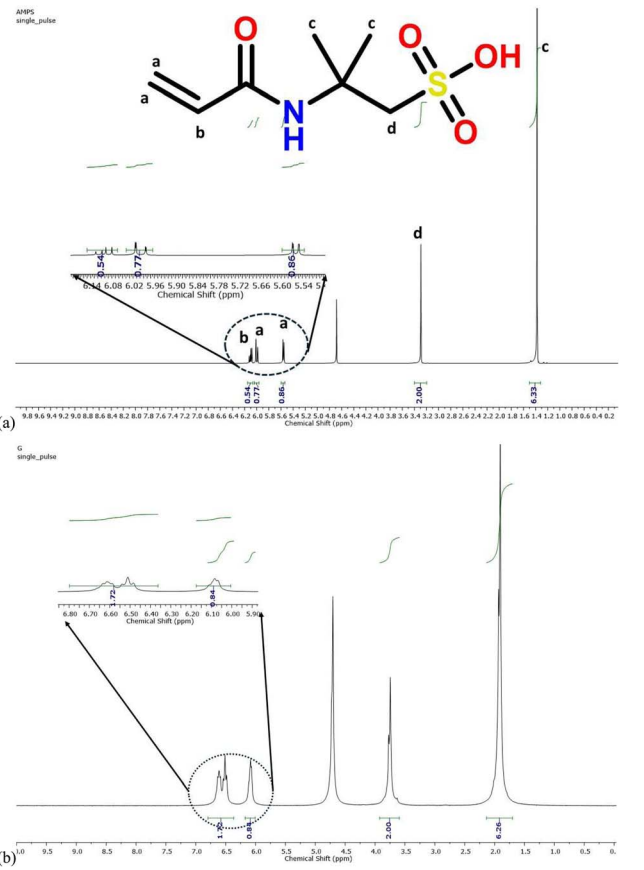

Fig. 3 ^{1}H NMR spectra of AMPS in D_2O at room temp. (a) and at 80 °C (b).

confirms that polymerization did not occur at 80 °C temperature. However, the spectral changes indicate modifications in the molecular environment of AMPS in solution. The temperature-dependent broadening and partial loss of the characteristic vinyl proton coupling patterns suggest enhanced intermolecular interactions and dynamic exchange processes. These effects likely arise from partial aggregation of AMPS molecules in aqueous media through hydrogen bonding involving the amide and sulfonic acid groups, together with strong hydration of the sulfonic acid functionality. Such interactions can lead to transient supramolecular assemblies in solution. These aggregates, in combination with water molecules, may establish hydrogen-bonded networks that facilitate proton exchange and proton mobility through Grotthuss-type mechanisms. Although direct proton transfer to the vinyl group cannot be detected by ^{1}H NMR, the observed spectral changes and variations in the HDO signal seem to suggest an active proton exchange process that modifies the local electronic environment of the vinyl group. Although this state alone is insufficient to initiate polymerization, it provides a microenvironment suitable for the polymerization.

The ESR spectra recorded at the X-band frequency are expected to exhibit the characteristic resonance of organic free radicals in the $g \approx 2.0$ region ($\approx$336 mT), confirming the formation of paramagnetic species. The spectra were acquired at 80, 120, 150, and 200 °C and are shown in Fig. S1 (SI). No detectable ESR signal was observed at 80 °C, indicating insufficient thermal activation for free radical formation. However, the progressive increase in signal intensity and improved spectral quality were observed at $\geq$120 °C, suggesting thermally induced radical formation in AMPS.

At 200 °C, the spectrum showed a distinct resonance when plotted as intensity *versus* *g*-value in Fig. 4, appearing as a broad signal centred at $g \approx 2.0$. This is a characteristic of carbon-centred organic radicals. Although hyperfine interactions with protons of the polymer backbone are expected, no resolved splitting is observed, probably due to motional averaging and thermal line broadening at elevated temperatures.

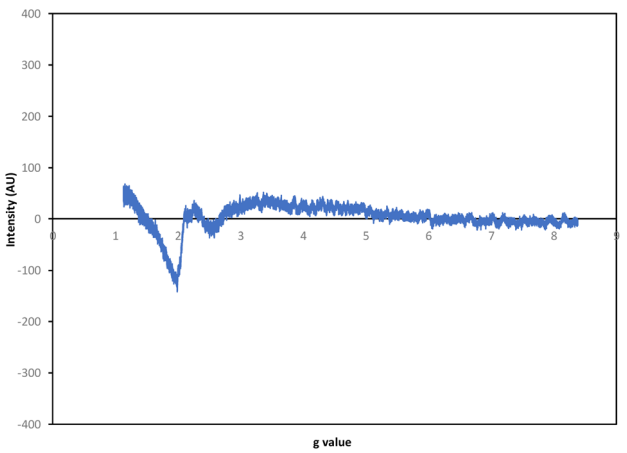

Fig. 4 ESR spectrum of AMPS in water at 200 °C recorded in the X-band frequency.

These results confirm the formation of thermally generated radicals along the AMPS backbone, with the unpaired electron exhibiting delocalized spin density. However, the temperature required for formation of free radicals on AMPS is higher, *i.e.* more than 120 °C.

3.3. Sono-mechanical activation

It has been shown that two primary effects that can originate from ultrasonic irradiation are mechanical forces (high shear) and chemical effects (radical formation).[23,24,40] The free radical formation during ultrasonication of an aqueous solution is negligible at low frequencies (*ca.* 20 kHz) and very high frequencies (>1 MHz), but in a good yield at 300–800 kHz.[23,24] To understand the free radical polymerization of AMPS, the free radical scavenger DPPH was used to inhibit polymerisation by sono-mechanical activation, and a radical scavenging assay (RSA) was carried out. EPR provides direct evidence of radical species, but the DPPH method is preferred as the DPPH assay is possible during sonication. However, the DPPH method is indirect and does not confirm that the free radicals are formed on AMPS by sonication. The DPPH method was used for *in situ* monitoring of the initiation of polymerization of methyl methacrylate with ultrasound.[41]

The radical scavenging activity (RSA) carried out using DPPH during the sonication of DI water with the same power and duration used in polymerization did not reveal the formation of free radicals in water to a significant extent. However, sonolysis of water with 20 kHz ultrasound may have generated OH$^{\bullet}$ and H$^{\bullet}$ radicals, but the yield might have been below the detection limit of RSA. It was observed that DPPH completely inhibited the formation of the crosslinked poly(AMPS) hydrogel by sonication (148 W cm^{-2} power) of an aqueous solution containing AMPS (2.4 mol L^{-1}) and 10 mol% cross-linker for 10 min, whereas the hydrogel formed readily within 5 min in the absence of DPPH. This suggested that the polymerisation of AMPS in the present case (20 kHz sonication) occurred due to cavitation. This was based on the fact that the radical scavenger DPPH was consumed in significant amounts (85–90%) during 5 min of sonication of an aqueous solution containing AMPS (2.4 mol L^{-1}) and AMPS (2.4 mol L^{-1}) with 10 mol% MBA, without any gel formation. Therefore, the primary source of radicals may have originated from AMPS or AMPS–water interactions under a sonication field rather than bulk water sonolysis. Direct mechanical stretching of a small vinyl bond in solution is unlikely. However, mechanical stress caused by cavitation may induce distortion and elongation of the protonated vinyl bond, facilitating homolytic cleavage.

3.4. Plausible mechanism of sono-polymerization

As discussed earlier for the polymerization of acrylamide in the presence of methanesulfonic acid and H_2SO_4, H^+ ions play a crucial role in enabling the direct generation of free radicals on the monomer. A similar proton-assisted activation pathway applies to AMPS. The NMR results indicate that thermal treatment creates a favourable microenvironment for polymerization. However, the ESR spectra reveal that significantly higher

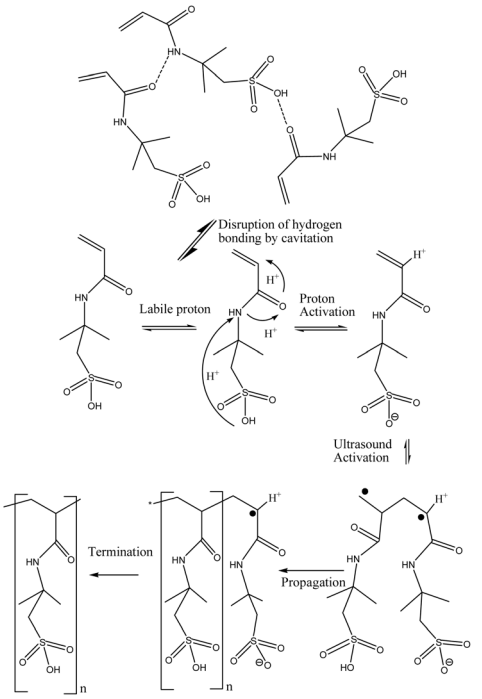

Fig. 5 The plausible mechanism of sono-mechanical polymerization of AMPS.

temperatures are required for the actual formation of monomer-centred radicals. This shows that thermal activation alone is insufficient for efficient radical generation in AMPS. Under 20 kHz sono-mechanical activation, the activation energy for radical formation is markedly reduced. The cavitation process at this frequency is governed primarily by thermal hotspots, shock waves, and microjet impacts, while water sonolysis remains negligible. The collapse of cavitation bubbles disrupts the hydrogen-bonded sulfonic acid clusters of AMPS, leading to the momentary release of labile protons. This localized proton surge induces transient protonation of the vinyl group, which polarizes the C=C bond and lowers the barrier for homolytic cleavage. Simultaneously, the applied mechanical stress stretches and distorts the protonated vinyl bond, promoting bond scission and generating monomer-centred radicals. FTIR analysis supports this mechanism by indicating the disappearance of the vinyl C=C stretching band that confirms polymerization, while the shifts in the amide and carbonyl regions indicate protonation and hydrogen-bond reorganization during activation. Once radicals are formed, chain propagation proceeds through successive radical addition to neighbouring monomer units, leading to the growth of the polymer backbone. Termination occurs either by radical recombination or by proton-mediated capping reactions. In this process, the sulfonic acid group performs dual functions, as a proton donor for activation and as a counterion for charge stabilization, thereby enabling an acid-assisted, hydrogen-bond-directed radical polymerization pathway. The sono-mechanical-based polymerization mechanism of AMPS could be explained by integrating proton activation, disruption of hydrogen-bonded clusters, and ultrasound-induced mechano-radical formation, as illustrated in Fig. 5.

3.5. Growth of poly(AMPS) chains

The free radical-initiated growth of poly(AMPS) was studied by measuring the viscosity of AMPS solution during sonication for different periods of time. Viscosity measurement is an effective method for monitoring the growth of AMPS polymer chains in water, as both the monomer and polymer are highly soluble in water, and the viscosity of the solution is directly correlated with the molecular weight and chain length. As polymerization progresses, the increasing chain length and entanglement lead to an increase in the viscosity of the polymerizing solution, providing real-time insight into polymerization kinetics. The variation of the viscosity of 20 mL solutions containing 0.6 and 0.8 mol L^{-1} as a function of sonication time at 148 W cm^{-2} power and 20 kHz frequency is shown in Fig. 6. It is seen from the curves for both AMPS concentrations that the viscosity increased initially and then decreased within 3 min. Again, the viscosity increased and reached a maximum at 5 min, then decreased to a minimum in 10 min. Thereafter, the viscosity increased continuously. For example, the viscosity of 0.6 mol L^{-1} reached 217 cP after 30 min, forming a highly viscous solution. These rise–fall cycles of viscosity and the continuous increase in viscosity suggested that the free radical polymerization of AMPS by sono-mechanical activation was governed by competing polymerization and depolymerization processes. Initially, during the first 5 min, the viscosity increased due to polymerization induced by sonication-generated free radicals, which promote chain growth and an increase in molecular weight. Between 5 and 15 minutes, the viscosity decreased as mechanical forces from cavitation caused chain scission, breaking polymer chains and reducing their molecular weight. However, after 15 minutes, polymerization dominated again due to the continued generation of free radicals, forming high-molecular-weight poly(AMPS) chains, which significantly increased the viscosity. This behaviour illustrated the dynamic balance between polymerization and depolymerization processes during sonication.

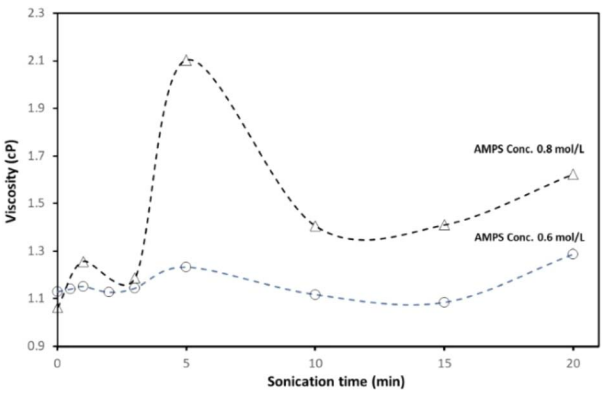

Fig. 6 The variation of viscosity of AMPS solutions as a function of sonication time with a constant power of 148 W cm^{-2} at 20 kHz.

Table 1 The molecular weights and polydispersity index of poly(AMPS) formed by sonication as obtained by GPC

Sample details	Peak (area)	M_n (g mol^{-1})	M_w (g mol^{-1})	PD
AMPS conc.: 0.8 mol L^{-1}; 10 min sonication at 148 W cm^{-2} and 20 kHz	1 (1.02%)	619	632	1.02
	2 (25.7%)	3677	3914	1.06
	3 (71.8%)	17 885	18 705	1.05
	4 (1.44%)	28 886	30 564	1.06
AMPS conc.: 0.8 mol L^{-1}; 20 min sonication at 148 W cm^{-2} and 20 kHz	1 (3.2%)	85	91	1.07
	2 (0.4%)	496	514	1.04
	3 (24.0%)	15 034	15 655	1.04
	4 (1.2%)	36 579	37 211	1.02
	5 (71.3%)	1 324 599	3 008 040	2.27

To study the formation of poly(AMPS) under sonication, the number average molecular weight (M_n), weight average molecular weight (M_w) and polydispersity index (PD) were determined by GPC for the samples sonicated for 10 min, where the viscosity was reduced as shown in Fig. 6, and for 20 min, leading to significant rise in the viscosity. The results obtained by GPC analyses are given in Table 1. It is seen from these results that there were multiple peaks of M_n. However, there were two major peaks of M_n in both samples. In the 10 min sonicated sample, the two major peaks of M_n were at 17 885 g mol^{-1} (72%) and 3677 g mol^{-1} (25%). Both the peaks had a PD close to 1. One major M_n peak grew to 1 324 599 g mol^{-1} (71%) and the PD was equal to 2.27, which are characteristics of free radical-based polymerization. Other peaks had low molecular weights. For example, the second major peak of M_n was 15 034 g mol^{-1} (25%) in the 20 min sonicated sample. This suggested that the small growing chains were added to the main growing chain, forming higher molecular weight chains and an increase in PD. The other peaks of M_n are attributed to fragments of polymer chains caused by cavitation.

In free radical polymerization by sono-mechanical activation, the simultaneous processes of polymerization (chain growth) and depolymerization (chain breaking) of poly(AMPS) led to multiple molecular weight peaks in GPC after 20 min of sonication. During polymerization, radical initiation and propagation resulted in chains of varying lengths, while termination through combination or disproportionation produced a broad molecular weight distribution. Depolymerization also occurred by cavitation, as seen by the rise and fall of viscosity shown in curves given in Fig. 6, where polymer chains broke into shorter fragments that could not undergo further polymerization. This process introduced additional low-molecular-weight species, further diversifying the molecular weight profile. In reversible radical systems, such as RAFT polymerization or thermal equilibrium conditions, polymerization and depolymerization can coexist dynamically, which was also observed in the sono-mechanical activation for different reasons. This equilibrium resulted in distinct high- and low-molecular-weight species, reflecting the balance between chain growth and fragmentation. Therefore, the appearance of multiple peaks in GPC could be attributed to the interplay of polymerization, depolymerization, and termination events. The formation of the hydrogel in a shorter time suggested that depolymerization did not play a significant role, and rapid crosslinking stabilized the three-dimensional network of the hydrogel. Contrary to this, chain growth free radical polymerization of poly(AMPS) involved propagation of long chains, which was inherently slower because it depended on the initiation and addition of individual monomers over a period of time. Therefore, shear forces could fragment the growing polymer chain.

3.6. Water uptake in hydrogels

Water uptake or swelling of hydrogels in water is important for biomedical and cementitious applications. The water uptake capacities of hydrogels are largely dependent on the network elasticity, which is correlated primarily with the crosslinking density and also with polymer chain flexibility to a certain extent. The sulfonic acid groups in poly(AMPS) contribute to

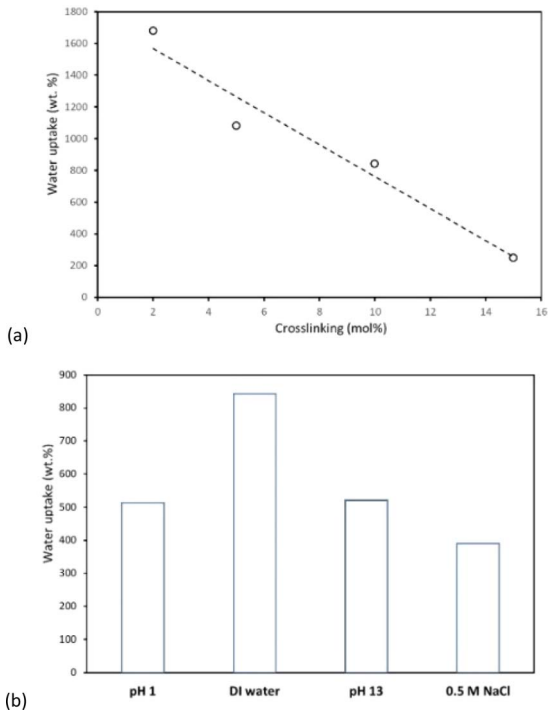

Fig. 7 Variation of the water uptake capacity of poly(AMPS) hydrogel as a function of crosslinking (mol% of MBA) (a) and the equilibrium water uptake capacity of 10 mol% crosslinked with poly(AMPS) in acid, base, DI water and salt (b).

high hydrophilicity, and, therefore, have flexible polymer chains, as can be seen from its chemical structure. Therefore, the crosslinking of poly(AMPS) is expected to have a major influence on its water uptake capacity. Fig. 7a shows that the poly(AMPS) hydrogel crosslinked with 2 mol% MBA exhibited a water uptake capacity of 1678 wt% in deionized water, indicating high hydrophilicity. However, the water uptake capacity decreased systematically with an increase of crosslinking in the poly(AMPS) hydrogel, *i.e.* reduced to 250 wt% at 15 mol% crosslinking. This seems to suggest that the desired water uptake capacity or swelling of the poly(AMPS) hydrogel could be obtained with the appropriate crosslinking extent.

It is also important to note that the water uptake capacity is also influenced by osmotic forces, which depend on the chemical conditions of the equilibrating solution. Therefore, the water uptake capacity of 10 mol% crosslinked poly(AMPS) was also studied in solutions having pH = 1, pH = 13 and 0.5 M NaCl and compared with that in deionized water. It is evident from Fig. 7b that the water uptake capacity followed the order: DI > pH = 1 ≈ pH = 13 > 0.5 NaCl. Thus, the equilibrium water uptake capacity of poly(AMPS) hydrogels crosslinked with a 10 mol% cross-linker varied significantly with the chemical composition of the equilibrating aqueous solution. The sulfonic acid group (–SO_3H) is a strong acidic group and therefore remains ionized at both acidic and basic pH. This led to similar water uptake capacity at lower and higher pHs. In salt solutions, however, the ions shield the charges on the –SO_3^- groups, reducing the electrostatic repulsion and osmotic pressure, resulting in significantly lower water uptake. The higher uptake capacity in DI water could be attributed to the higher osmotic pressure in the poly(AMPS) hydrogel and no charge shielding.

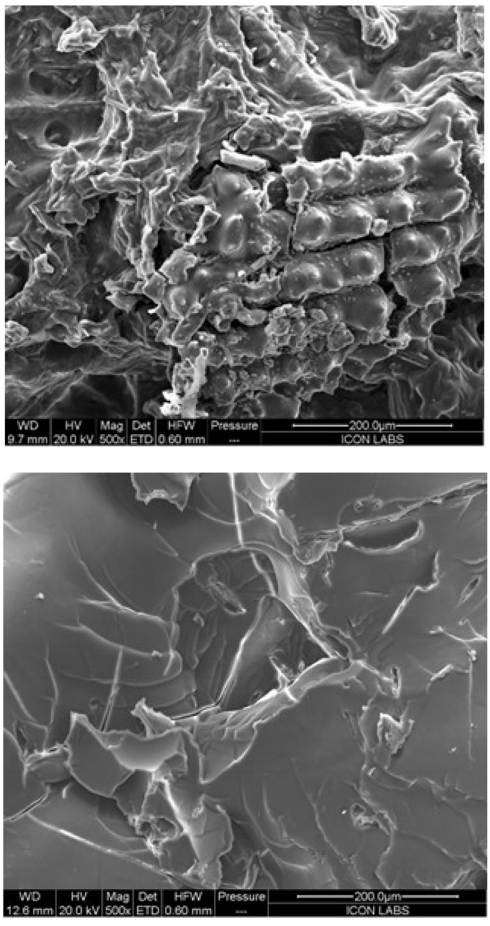

Fig. 8 Representative FESEM images of the crosslinked poly(AMPS) hydrogel formed by using polymerizing solutions having AMPS concentrations of 2.4 mol L^{-1} (a) and 1.4 mol L^{-1} (b) under similar conditions.

3.7. Characterization of poly(AMPS)

The physical structures of MBA-crosslinked poly(AMPS) hydrogels prepared under identical conditions but with varying concentrations of AMPS monomer were examined using FESEM. Representative FESEM images of two hydrogels, synthesized from 2.4 mol L^{-1} and 1.4 mol per L AMPS and 10 mol% MBA in polymerizing solutions under ultrasound irradiation (20 kHz and 148 W cm^{-2}), are shown in Fig. 8. It is seen from the FESEM images shown in Fig. 8 that the gel formed with a higher concentration had fragmented structures with non-uniform density. In contrast, the gel formed by a dilute AMPS solution exhibited a uniform monolith with a non-porous structure. The crosslinked poly(AMPS) hydrogels formed at higher monomer concentrations were non-uniform and fragmented due to rapid polymerization and crosslinking, which led to localized gelation, phase separation, and mechanical stresses during solidification. The fast reaction kinetics created porous structures and irregularities, as monomers and cross-linkers were consumed unevenly. In contrast, lower monomer concentrations resulted in controlled polymerization, allowing uniform diffusion of monomers and crosslinkers. This produced a homogeneous, dense, and non-porous hydrogel with reduced internal stresses. The slower reaction prevented void formation and ensured structural uniformity. The FESEM images of the same crosslinked poly(AMPS) hydrogel loaded with Ca^{2+} did not show physical changes due to additional ionic crosslinking, see Fig. S2 (SI). The EDS spectrum shows the presence of the peaks of C, O, N, and S atoms, as expected from the chemical structures of AMPS and MBA, see Fig. S3 (SI).

The chemical structure of crosslinked poly(AMPS) was confirmed by studying its FTIR spectrum and comparing it with the FTIR spectra of the monomer AMPS and the crosslinker MBA. The FTIR spectra are given in Fig. S4 (SI). It is seen from the FTIR spectrum of the poly(AMPS) hydrogel shown in Fig. S4c (SI) that characteristic peaks corresponding to the amide group (N–H stretch: the broad peak around 3330 cm^{-1}, C═O stretch: the strong peak near 1645 cm^{-1}, and N–H bend: the peak near 1550 cm^{-1}) and sulfonic acid group (S═O stretch: two strong peaks near 1039–1181 cm^{-1} and smaller peaks due to shift caused by hydrogen bonding with water) were present. The C═C stretching peak at 1612 cm^{-1}, characteristic of the vinyl double bond in AMPS and MBA, disappeared in the poly(AMPS) hydrogel. Instead, a new peak appeared in the FTIR spectrum of the hydrogel at 1391 cm^{-1} due to C–N stretching vibrations from the MBA crosslinker. Thus, the FTIR spectrum

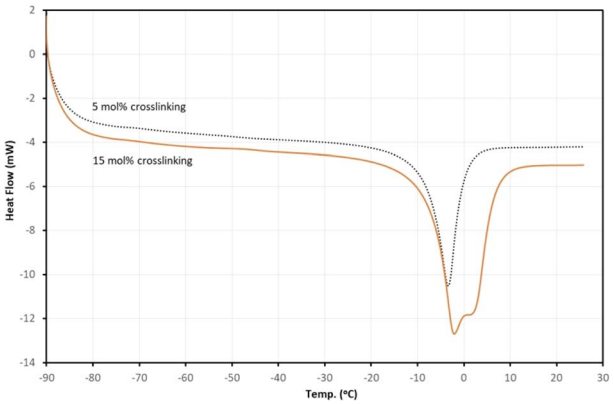

Fig. 9 DSC curves of poly(AMPS) crosslinked with 5 mol% (dashed line) and 15 mol% (solid line) of MBA.

comparison indicated that the expected chemical structure of the hydrogel was formed, and there was no degradation of the monomer and crosslinker during sonication.

The DSC thermograms of poly(AMPS) hydrogels crosslinked with 5 mol% and 15 mol% MBA given in Fig. 9 show characteristic thermal transitions associated with water melting and glass transition of the polymer network. It is seen for the 5 mol% MBA-crosslinked poly(AMPS) hydrogel that a single broad endothermic peak is observed in the sub-zero (−27 °C) to near-zero (8 °C) temperature region and a peak at −3.5 °C. This endothermic thermal transition could be attributed to the melting of freezable water confined within the hydrogel network as well as T_g. The broad nature of this peak indicates a distribution of water environments, primarily dominated by loosely bound or free water, weakly interacting with the sulfonate ($-SO_3^-$) groups of poly(AMPS). In contrast, the 15 mol% MBA crosslinked hydrogel exhibited two partially overlapped endothermic peaks in the water-melting region. This behavior suggests the presence of two distinct water domains within the highly crosslinked network. This first endothermic transition could be attributed to free or weakly bound water, melting closer to 0 °C. The second endothermic transition is due to more strongly bound or confined water, associated with ionic interactions and nanoscale confinement imposed by the dense crosslinking. The increased crosslink density restricts chain mobility and creates heterogeneous microdomains, leading to separation of water environments and peak splitting. It is also possible that the T_g of poly(AMPS) hydrogel with 15 mol% MBA shifts to a higher temperature and becomes broader due to restricted segmental motion, which may merge with the bound-water endotherm, resulting in the observed joined peaks. It is interesting to note that the DSC curve of the 15 mol% crosslinked hydrogel shows a more negative baseline shift compared to the 5 mol% sample. This feature is indicative of enhanced network rigidity, consistent with increased crosslink density and reduced polymer chain mobility. The stronger polymer–water interactions and higher fraction of non-freezable or strongly bound water further contribute to this baseline shift. The DSC results suggested that increasing MBA content from 5 to 15 mol% significantly alters the thermal behavior, water–polymer interactions, and microstructural heterogeneity of poly(AMPS) hydrogels.

The thermal properties of 5% MBA-crosslinked poly(AMPS) under a nitrogen atmosphere were studied by thermogravimetric analysis (TGA) and differential thermal analysis (DTA). The degradation pathway of crosslinked poly(AMPS) under N_2 is expected to be an endothermic transition corresponding to dehydration and exothermic thermal transitions attributed to desulfonation of $-SO_3H$ groups, amide linkage decomposition, main-chain scission and carbonaceous char formation. The TGA and DTA curves given in Fig. S5a and b (SI) exhibit a multistep degradation pattern as expected. An initial weight loss of ∼14.6% below 150 °C corresponds to the removal of free and hydrogen-bonded water, consistent with the broad endothermic DTA peak in the corresponding region. The second degradation stage (150–300 °C) could be attributed to the degradation of $-SO_3H$ groups coincident with the release of strongly bound water. The major exothermic peaks at ∼279 °C and ∼326 °C in the DTA curve coincided with mass loss and could be assigned to sulfonic acid decomposition, followed by amide group cleavage and main-chain scission of the AMPS backbone. A minor thermal transition near 396 °C corresponded to secondary degradation and carbonization processes. The residual mass at high temperature indicated char formation.

3.8. Self-healing of hydrogels

Su *et al.* have reported the preparation of poly(AMPS) hydrogel *via* UV polymerization, and, unlike chemical crosslinking, this gel was stabilized in water by H-bonding.[42] This hydrogel showed high water uptake capacity and good self-healing efficiency. The 2 mol% crosslinked poly(AMPS) hydrogel prepared by sono-mechanical activation also showed high water uptake capacity. Therefore, this gel may also have self-healing properties. To study the self-healing ability of hydrogel, the 2 mol% crosslinked poly(AMPS) sample was cut into two equal parts using a sharp blade. The half-cut portion of the hydrogel was equilibrated with a water solution of cationic dye methylene blue, which was loaded by an ion-exchange process. The unbound methylene blue dye was removed by washing with excess water. The cut pieces were carefully aligned and rejoined at the cut interface without applying external force and kept for 24 h under humid conditions and also under ambient conditions. It is seen from Fig. 10 that the two cut pieces were joined in 24 h, indicating the self-healing properties of 2 mol% crosslinked poly(AMPS) hydrogel under humid as well as ambient conditions. This could be attributed to the fact that the hydrogel contained significant water content, which acted as a plasticizer. This allowed polymer chains sufficient mobility to diffuse across a damaged region and reconnect *via* hydrogen bonding interactions, as the poly(AMPS) hydrogel consisted of hydrogen bonding carbonyl, amide and sulfonic groups. Also, sufficient mobility of polymer chains due to lower crosslinking would allow redistribution and entanglement of polymer chains at the adjoining interface of two cut pieces of hydrogel.

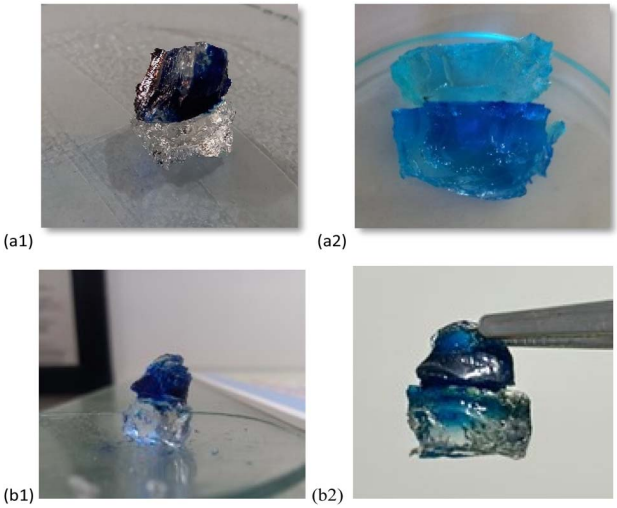

Fig. 10 Images showing two cut pieces of poly(AMPS) hydrogel (2 mol% crosslinking), one blank and another loaded with methylene blue: before self-healing (a1) and after self-healing for 24 h under humid conditions (a2); before self-healing (b1) and after 24 h of self-healing (b2) under ambient conditions.

It is important to note from Fig. 10a2 that the methylene blue dyes diffused in the unloaded cut piece under humid conditions but not in the hydrogel gel piece dried under ambient conditions, as can be seen from Fig. 10b2. This could be due to high chain mobility in the hydrogel with higher water content, which would allow the proximity of fixed binding sites. Methylene blue binds to fixed sulfonate sites *via* reversible ionic bonds, allowing exchange with nearby sulfonate groups. This would lead to the diffusion of bound methylene blue from one binding site to another binding site by jumping[43] and lead to the uniform distribution of methylene blue in both cut pieces. However, this would not be possible when the water content is lower, leading to insufficient chain mobility required for the fixed-site jumping.

The process of self-healing in the lightly crosslinked poly(-AMPS) involves true network reformation rather than surface sticking alone. This is based on the fact that when two cut hydrogel pieces, one loaded with MB, were brought into contact, the diffusion of the dye across the interface occurred after fusion overnight. Such interfacial molecular exchange requires the presence of water-swollen, dynamic polymer chains capable of interpenetration and reorganization, which is not consistent with mere surface adhesion. The microscopic observations show a gradual disappearance of the interface and reconstitution of a continuous network, supporting a self-healing mechanism driven by chain mobility and reversible hydrogen bonding interactions within the lightly crosslinked AMPS hydrogel matrix. The dye-diffusion experiment and the visualization demonstrate that the healing process arises from chain interdiffusion and network relaxation, rather than simple physical adhesion.

3.9. Application in Portland cement

The incorporation of functional polymeric materials into cementitious systems has emerged as an effective strategy for modifying hydration behavior, mechanical performance, and microstructural development.[44,45] The polymer hydrogels have been used for immobilizing bacterial spores and chemical reagents for imparting self-healing properties to cement and concrete materials.[45] However, the chemical composition of the hydrogel is important as it significantly affects the hydration chemistry of the cement, resulting in lower mechanical performance of the cementitious materials.[45] In the present work, Ca-poly(AMPS) was used as the additive in ordinary Portland cement (OPC). It was expected that the crosslinked poly(AMPS) hydrogel would function as a multifunctional additive, regulating hydration kinetics, providing water for internal curing, and enhancing the crack resistance without compromising long-term structural integrity. The use of the calcium form of poly(AMPS) is particularly important for cement compatibility. In its acidic (H^+) form, poly(AMPS) contains strongly acidic sulfonic groups that significantly lower the compressive strength of the cement.[46] The acidic sulfonic acid groups retard cement hydration by lowering the pore solution pH and complexing with Ca^{2+} ions released during the dissolution of clinker phases. Conversion to the Ca-form neutralizes the acid functionality and pre-saturates the sulfonate groups with Ca^{2+} ions. Small dosages of crosslinked Ca-poly(AMPS), ranging from 0.3 to 2 wt% of cement, were incorporated, and the setting time, heat of hydration, and compressive and tensile strengths of OPC were evaluated as given in the Experimental section. The crosslinking extents of Ca-poly(AMPS) were 5, 10 and 15 mol%. The results obtained are summarized in Table 2.

The Ca-poly(AMPS) hydrogel contains calcium sulfate species, which are chemically analogous to gypsum commonly added to OPC to regulate the hardening process. In view of this similarity, both initial and final setting times were systematically evaluated. The results indicate that incorporation of the hydrogel exerts only a marginal influence on the initial setting time, which remains close to that of the control mixture (approximately 140–151 min). In contrast, the final setting time exhibits a moderate increase with increasing hydrogel dosage, reaching up to 239 min in certain formulations. The variation of setting times with dosage for the 15 mol% crosslinked Ca-poly(AMPS) system shown in Fig. 11 suggests that, at the maximum dosage of 2 wt%, the initial setting time decreases by about 7%, whereas the final setting time increases by approximately 10% relative to the control. The slight acceleration of the initial set may be attributed to the availability of additional calcium ions that promote early ettringite formation,[46] while the moderate retardation of the final set likely arises from regulated release of water from the hydrogel network. Importantly, both the acceleration of the initial setting and the retardation of the final setting remain within acceptable practical limits for cementitious applications.

The cumulative heat of hydration data given in Table 2 suggests the hydration-regulating function of the hydrogel. At 7 days, total heat release is slightly lower for hydrogel-containing systems (approximately 285–296 kJ kg^{-1}) compared with the control (298 kJ kg^{-1}), indicating moderated early hydration kinetics. The reduction in early heat evolution is beneficial for

Table 2 Comparison of the mechanical performance, heat of hydration, and setting characteristics of Ordinary Portland Cement modified with different dosages (0.3–2.0 wt%) of Ca-poly(AMPS) hydrogels having varying crosslinking densities (5–15 mol%)

Crosslinking (mol%)	Dose (wt%)	Compressive strength (MPa)			Tensile strength (MPa)			Heat of hydration (kJ kg^{-1})			Setting time (min)	
		7 days	28 days	60 days	7 days	28 days	60 days	7 days	28 days	60 days	Initial	Final
Control	0	35 ± 2	48 ± 3	57 ± 5	2.9 ± 0.2	3.5 ± 0.3	4.2 ± 0.4	298 ± 9	335 ± 11	347 ± 15	150 ± 15	210 ± 10
5	0.3	33 ± 3	43 ± 3	52 ± 5	2.9 ± 0.2	3.6 ± 0.3	4.3 ± 0.4	295 ± 9	334 ± 11	343 ± 15	148 ± 15	220 ± 10
	0.5	32 ± 3	40 ± 3	52 ± 5	2.9 ± 0.2	3.4 ± 0.3	4.1 ± 0.4	293 ± 9	332 ± 11	343 ± 15	145 ± 15	226 ± 10
	1.0	33 ± 3	41 ± 3	49 ± 5	2.7 ± 0.2	3.7 ± 0.3	4.3 ± 0.4	291 ± 9	330 ± 11	346 ± 15	141 ± 15	227 ± 10
	2.0	29 ± 3	42 ± 3	50 ± 5	3.0 ± 0.2	3.6 ± 0.3	4.3 ± 0.4	287 ± 9	329 ± 11	342 ± 15	140 ± 15	231 ± 10
10	0.3	34 ± 3	43 ± 3	51 ± 5	2.9 ± 0.2	3.8 ± 0.3	4.4 ± 0.4	296 ± 9	334 ± 11	345 ± 15	151 ± 15	212 ± 10
	0.5	31 ± 3	40 ± 3	50 ± 5	3.0 ± 0.2	3.6 ± 0.3	4.5 ± 0.4	293 ± 9	331 ± 11	341 ± 15	149 ± 15	218 ± 10
	1.0	32 ± 3	40 ± 3	51 ± 5	3.0 ± 0.2	3.7 ± 0.3	4.6 ± 0.4	291 ± 9	330 ± 11	345 ± 15	143 ± 15	225 ± 10
	2.0	30 ± 3	41 ± 3	50 ± 5	3.1 ± 0.2	3.8 ± 0.3	4.6 ± 0.4	287 ± 9	329 ± 11	342 ± 15	146 ± 15	234 ± 10
15	0.3	33 ± 3	42 ± 3	50 ± 5	3.0 ± 0.2	3.7 ± 0.3	4.4 ± 0.4	291 ± 9	330 ± 11	338 ± 15	149 ± 15	223 ± 10
	0.5	31 ± 3	40 ± 3	51 ± 5	3.0 ± 0.2	3.7 ± 0.3	4.3 ± 0.4	291 ± 9	332 ± 11	334 ± 15	148 ± 15	225 ± 10
	1.0	31 ± 3	42 ± 3	51 ± 5	2.9 ± 0.2	3.7 ± 0.3	4.5 ± 0.4	290 ± 9	328 ± 11	348 ± 15	151 ± 15	227 ± 10
	2.0	29 ± 3	41 ± 3	49 ± 5	3.1 ± 0.2	3.7 ± 0.3	4.7 ± 0.4	285 ± 9	327 ± 11	341 ± 15	145 ± 15	239 ± 10

minimizing thermal gradients and associated cracking risks in mass concrete applications. However, at later ages, the differences in cumulative heat become marginal, confirming that total hydration is not suppressed but temporally redistributed.

The incorporation of the crosslinked poly(AMPS) hydrogel into OPC is expected to influence the mechanical performance depending upon the crosslinking density and dosage. It is seen from Table 2 that a consistent but moderate reduction in early-age compressive strength is observed in all hydrogel-containing systems compared with the control mix. At 7 days, compressive strength decreased from 35 MPa for the control to values in the range of 29–34 MPa depending on hydrogel content. This early reduction can be attributed primarily to a localized decrease in free water availability for immediate cement hydration. Additionally, the swollen hydrogel domains may introduce early capillary porosity. Despite this initial reduction, strength development at later ages shows substantial recovery. At 28 and 60 days, compressive strength values approach those of the control system, reaching 49–52 MPa at 60 days compared to 57 MPa for neat OPC. This convergence indicates that the hydrogel does not permanently inhibit hydration. However, it redistributes the hydration process over time. As the internal relative humidity decreases during ongoing hydration, the hydrogel gradually releases stored water, enabling continued reaction of unhydrated clinker phases. This internal curing mechanism promotes secondary formation of the C–S–H gel, contributing to progressive matrix densification and partial compensation for early porosity. In contrast to compressive strength, tensile strength is maintained or slightly improved in hydrogel-modified systems, particularly at later curing ages. Values up to 4.6–4.7 MPa at 60 days are observed compared with 4.2 MPa for the control, see Table 2. The improved tensile response suggests that the hydrogel contributes to stress redistribution and microcrack control within the cementitious matrix. The polymeric domains may act as localized energy-dissipating centres, reducing crack propagation and enhancing resistance to tensile stresses. This behavior is particularly important for durability performance, where crack control is requisite.

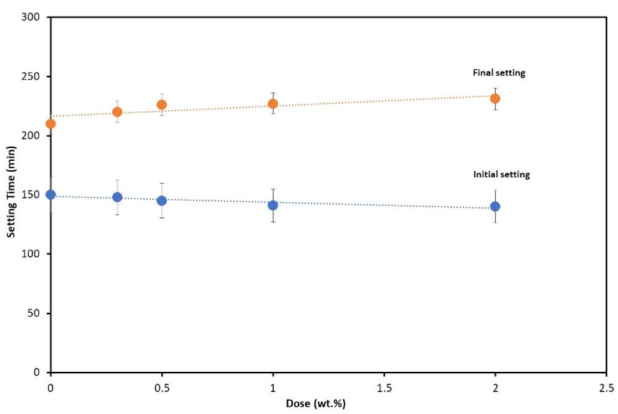

Fig. 11 Variation of initial and final setting times of Ordinary Portland Cement as a function of dosage of 15 mol% MBA crosslinked Ca-poly(AMPS) hydrogel.

4. Conclusions

The present study demonstrates a sono-mechanical activation-assisted, proton-catalyzed self-polymerization of AMPS in aqueous medium under ambient conditions. Variable-temperature ^{1}H NMR spectra revealed pronounced line broadening at elevated temperatures, indicating aggregation and restricted molecular mobility of AMPS in water. Such aggregation creates a favorable microenvironment for proton-assisted activation but does not itself leads to polymerization. In contrast, ESR measurements clearly showed that thermal activation (≥120 °C) is required to generate detectable organic free radicals on the AMPS monomer, establishing that purely thermal self-initiation demands significant activation energy. High-intensity, low-frequency ultrasound (20 ± 3 kHz) effectively lowered this activation barrier, enabling self-polymerization under ambient conditions. The sono-mechanical effect is attributed to acoustic cavitation, which

generates localized hot spots, high shear forces, and enhanced proton mobility (proton hopping) in water. Notably, polymerization occurred only in aqueous medium and not in deep eutectic solvent systems or when H^+ was replaced by Na^+ ions, confirming the essential role of protonation. These findings support a mechanism in which intramolecular protonation of the vinyl group by the $–SO_3H$ functionality promotes H^+-assisted radical self-initiation, but requires sufficient energy to overcome the activation barrier, which is substantially reduced under ultrasonic irradiation in water. MBA-crosslinked poly(-AMPS) hydrogels exhibited tunable swelling behavior governed by the crosslink density, pH, and ionic strength, along with intrinsic self-healing due to reversible hydrogen bonding and ionic interactions. Thermal analyses (TGA, DTA, and DSC) confirmed structural integrity and stability. Initial endothermic transitions in TGA/DTA correspond to free and bound water loss, while exothermic events at higher temperatures are associated with desulfonation and backbone degradation, verifying the formation of a stable crosslinked network suitable for cementitious environments. DSC further indicated the presence of two distinct water microdomains at a higher crosslink density (15 mol%), reflecting heterogeneous water structuring within the hydrogel matrix. Upon conversion to Ca-poly(AMPS) and incorporation into Ordinary Portland Cement, the hydrogel functions as an internal curing agent and a self-healing agent. It absorbs mixing water and gradually releases it during hydration, sustaining C–S–H formation and enhancing later-age strength. Although early compressive strength is marginally reduced due to moderated hydration kinetics, long-term strength recovery was substantial, and tensile performance was maintained or slightly improved. The swelling capacity enables autogenous crack sealing upon water ingress, promoting secondary hydration and durability enhancement. Importantly, modifications in initial and final setting times remain within practical limits. In general, the developed hydrogel offers strong potential for internal curing, durability enhancement, and immobilization of bacterial or chemical self-healing agents in cementitious systems.

Author contributions

Kuldeep Rajpurohit: data curation, investigation, methodology, validation. Sabrina A. Shaikh: formal analysis, methodology, software, validation. Ashok K. Pandey: conceptualization, validation, visualization, writing – original draft. Hemlata K. Bagla: conceptualization, resources, supervision, writing – review & editing.

Conflicts of interest

There are no conflicts to declare.

Data availability

The data supporting this article have been included as part of the supplementary information (SI). Supplementary information: ESR spectra of AMPS in water at room temperature, 80 °C, 120 °C, 150 °C, and 200 °C; FESEM images of Ca^{2+}-loaded crosslinked poly(AMPS) hydrogel; EDS of crosslinked poly(-AMPS) hydrogel; FTIR Spectra of monomer AMPS, crosslinker MBA, and crosslinked poly(AMPS) hydrogel; the thermogravimetric analysis (TGA) and differential thermal analysis (DTA) of 5% MBA-crosslinked poly(AMPS) under nitrogen atmosphere; formation of hydrogel using 2.4 mol L^{-1} monomer (10 mL) with 10 mol% MBA under ultrasound irradiation (20 kHz, 148 W cm^{-2}); and Experimental section. See DOI: https://doi.org/10.1039/d5mr00122f.

Acknowledgements

The authors are thankful to SAIF, IIT-Bombay, Mumbai, India, for carrying out NMR, ESR, FESEM, DSC and TGA. Authors are thankful to Tanmaya Das, Department of Chemistry, IIT Kharagpur for help in proton NMR studies. Kuldeep Rajpurohit and Dr Sabrina A. Shiakh are thankful to HSNC University, Mumbai, for providing financial assistance.

Notes and references

1 N. Kumar, R. Gusain, S. Pandey and S. S. Ray, Hydrogel nanocomposite adsorbents and photocatalysts for sustainable water purification, *Adv. Mater. Interfaces*, 2023, **10**, 2201375, DOI: 10.1002/admi.202201375.
2 Y. Guo and G. Yu, Engineering hydrogels for efficient solar desalination and water purification, *Acc. Mater. Res.*, 2021, **2**, 374–384, DOI: 10.1021/accountsmr.1c00057.
3 Y. Guo, J. Bae, F. Zhao and G. Yu, Functional hydrogels for next-generation batteries and supercapacitors, *Trends Chem.*, 2019, **1**(3), 335–348, DOI: 10.1016/j.trechm.2019.03.005.
4 Y. Guo, J. Bae, Z. Fang, P. Li, F. Zhao and G. Yu, Hydrogels and Hydrogel-derived materials for energy and water sustainability, *Chem. Rev.*, 2020, **120**, 7642–7707, DOI: 10.1021/acs.chemrev.0c00345.
5 S. Shakiba, C. E. Astete, S. Paudel, C. M. Sabliov, D. F. Rodrigues and S. M. Louie, Emerging investigator series: polymeric nanocarriers for agricultural applications: synthesis, characterization, and environmental and biological interactions, *Environ. Sci.: Nano*, 2020, **7**, 37–67, DOI: 10.1039/c9en01127g.
6 C. Qin, H. Wang, Y. Zhao, Y. Qi, N. Wu, S. Zhang and W. Xu, Recent advances of hydrogel in agriculture: Synthesis, mechanism, properties and applications, *Eur. Polym. J.*, 2024, **219**, 113376, DOI: 10.1016/j.eurpolymj.2024.113376.
7 J. A. Hunt, R. Chen, T. van Veen and N. Bryan, Hydrogels for tissue engineering and regenerative medicine, *J. Mater. Chem. B*, 2014, **2**(33), 5319–5338, DOI: 10.1039/C4TB00775A.
8 J. Li, X. Jia and L. Yin, Hydrogel: diversity of structures and applications in food science, *Food Rev. Int.*, 2021, **37**(3), 313–372, DOI: 10.1080/87559129.2020.1858313.
9 D. Buenger, F. Topuz and J. Groll, Hydrogels in sensing applications, *Prog. Polym. Sci.*, 2012, **37**(12), 1678–1719, DOI: 10.1016/j.progpolymsci.2012.09.001.

10 B. Zhu, Q. Li, W. Zou and W. Chen, A novel method of self-healing in cementitious materials by using polyacrylic hydrogel, *KSCE J. Civ. Eng.*, 2020, **24**, 3406–3415, DOI: 10.1007/s12205-020-0090-6.

11 L. Peng, Y. An, H. Xiang, X. Pan, Y. Wang, Q. Yang, X. Cao, Z. L. Wang and L. Zhang, Liquid metal complexing Fe_3O_4 nanoparticles enable rapid polymerization of magnetically conductive hydrogels for various flexible electronics, *Nano Energy*, 2024, **130**, 110058, DOI: 10.1016/j.nanoen.2024.110058.

12 S. Das, A. K. Pandey, A. A. Athawale and V. K. Manchanda, Adsorptive preconcentration of uranium in hydrogels from seawater and aqueous solutions, *Ind. Eng. Chem. Res.*, 2009, **48**, 6789–6796, DOI: 10.1021/ie801912n.

13 S. Chappa, S. Das, A. K. Debnath, M. Sahu, M. K. Saxena and A. K. Pandey, Spacer monomer in polymer chain influencing affinity of ethylene glycol methacrylate phosphate toward UO_2^{2+} and Pu^{4+} ions, *Ind. Eng. Chem. Res.*, 2016, **55**, 8992–9002, DOI: 10.1021/acs.iecr.6b01534.

14 F. Acciaretti, S. Vesentini and L. Cipolla, Fabrication strategies towards hydrogels for biomedical application: chemical and mechanical insights, *Chem.–Asian J.*, 2022, **17**, e202200797, DOI: 10.1002/asia.202200797.

15 E. M. Ahmed, Hydrogel: preparation, characterization, and applications: A review, *J. Adv. Res.*, 2015, **6**, 105–121, DOI: 10.1016/j.jare.2013.07.006.

16 J. Yang, L. Rao, Y. Wang, Y. Zhao, D. Liu, Z. Wang, L. Fu, Y. Wang, X. Yang, Y. Li and Y. Liu, Recent advances in smart hydrogels prepared by ionizing radiation technology for biomedical applications, *Polymers*, 2022, **14**, 4377, DOI: 10.3390/polym14204377.

17 A. Krusenbaum, S. Grätz, G. T. Tigineh, L. Borchardt and J. G. Kim, The mechanochemical synthesis of polymers, *Chem. Soc. Rev.*, 2022, **51**, 2873–2905, DOI: 10.1039/d1cs01093j.

18 S. Akbulatov and R. Boulatov, Experimental polymer mechanochemistry and its interpretational frameworks, *ChemPhysChem*, 2017, **18**, 1422–1450, DOI: 10.1002/cphc.201601354.

19 H. Feng, X. Shao and Z. Wang, Mechanochemical controlled radical polymerization: From harsh to mild, *ChemPlusChem*, 2024, **89**, e202400287, DOI: 10.1002/cplu.202400287.

20 K. S. Suslick, Sonochemistry, *Science*, 1990, **247**(4949), 1439–1445, DOI: 10.1126/science.247.4949.1439.

21 K. S. Suslick, Mechanochemistry and sonochemistry: concluding remarks, *Faraday Discuss.*, 2014, **170**, 411–422, DOI: 10.1039/c4fd00148f.

22 A. K. Pandey, P. C. Kalsi and R. H. Iyer, Effects of high intensity ultrasound in chemical etching of particle tracks in solid state nuclear track detectors, *Nucl. Instrum. Methods Phys. Res., Sect. B*, 1998, **134**, 393–399.

23 T. G. McKenzie, F. Karimi, M. Ashokkumar and G. G. Qiao, Ultrasound and sonochemistry for radical polymerization: Sound synthesis, *Chem.–Eur. J.*, 2019, **25**, 5372–5388, DOI: 10.1002/chem.201803771.

24 A. R. S. Santha Kumar, A. Padmakumar, U. Kalita, S. Samanta, A. Baral, N. K. Singha, M. Ashokkumar and G. G. Qiao, Ultrasonics in polymer science: applications and challenges, *Prog. Mater. Sci.*, 2023, **136**, 101113, DOI: 10.1016/j.pmatsci.2023.101113.

25 G. Cravotto, E. C. Gaudinoa and P. Cintas, On the mechanochemical activation by ultrasound, *Chem. Soc. Rev.*, 2013, **42**, 7521–7534, DOI: 10.1039/c2cs35456j.

26 M. A. Bradley, S. W. Prescott, H. A. S. Schoonbrood, K. Landfester and F. Grieser, Miniemulsion Copolymerization of Methyl Methacrylate and Butyl Acrylate by Ultrasonic Initiation, *Macromolecules*, 2005, **38**, 6346–6351, DOI: 10.1021/ma0473622.

27 J. Prabha, W. S. Jemima, M. Jayaprada and M. J. Umapathy, Synergistic effect of ultrasonication and phase transfer catalysts in radical polymerization of methyl methacrylate - A kinetic study, *Ultrason. Sonochem.*, 2017, **35**, 333–341, DOI: 10.1016/j.ultsonch.2016.10.011.

28 K. Sankar and V. Rajendran, Ultrasound assisted free radical polymerization of glycidyl methacrylate by a new disite phase-transfer catalyst system: A kinetic study, *Ultrason. Sonochem.*, 2012, **19**(6), 1205–1212, DOI: 10.1016/j.ultsonch.2012.01.015.

29 P. Cass, W. Knower, E. Pereeia, N. P. Holmes and T. Hughes, Preparation of hydrogels via ultrasonic polymerization, *Ultrason. Sonochem.*, 2010, **17**, 326–332, DOI: 10.1016/j.ultsonch.2009.08.008.

30 B. Rokita, J. M. Rosiak and P. Ulanski, Ultrasound-induced cross-linking and formation of macroscopic covalent hydrogels in aqueous polymer and monomer solutions, *Macromolecules*, 2009, **42**(9), 3269–3274, DOI: 10.1021/ma802565p.

31 Y. Qi, H. Shao, D. Luo, L. Xiang, J. Luo, Q. Tian and S. Qin, Antifouling poly(vinylidene fluoride) hollow fiber membrane with hydrophilic surfaces by ultrasonic wave-assisted graft polymerization, *Polym. Eng. Sci.*, 2019, **59**, E446–E454, DOI: 10.1002/pen.25012.

32 H. Shao, Y. Qi, S. Liang, S. Qin and J. Yu, Polypropylene composite hollow fiber ultrafiltration membranes with an acrylic hydrogel surface by in situ ultrasonic wave-assisted polymerization for dye removal, *J. Appl. Polym. Sci.*, 2019, **136**, 47099, DOI: 10.1002/app.47099.

33 H. Shao, F. Wei, D. Luo, K. Zhang, S. Liang, Q. Tian, S. Qin and J. Yu, Improving the antifouling property of polypropylene hollow fiber membranes by in situ ultrasonic wave-assisted polymerization of styrene and maleic anhydride, *Polym. Eng. Sci.*, 2019, **59**, E51–E58, DOI: 10.1002/pen.24843.

34 W. Brand-Williams, M. E. Cuvelier and C. Berset, Use of a free radical method to evaluate antioxidant activity, *LWT – Food Sci. Technol.*, 1995, **28**(1), 25–30, DOI: 10.1016/S0023-6438(95)80008-5.

35 L. S. Chua, N. L. A. Rahaman, N. A. Adnan and T. T. E. Tan, Antioxidant activity of three honey samples in relation with their biochemical components, *J. Anal. Methods Chem.*, 2013, 313798, DOI: 10.1155/2013/313798.

36 Bureau of Indian Standards, *IS 4031 (Part 9): 1988, Methods of Physical Tests for Hydraulic Cement – Part 9: Determination of Heat of Hydration*, BIS, New Delhi, India.

37 Bureau of Indian Standards, *IS 4031 (Part 5): 1988, Methods of Physical Tests for Hydraulic Cement – Part 5: Determination of Initial and Final Setting Times*, BIS, New Delhi, India.
38 Bureau of Indian Standards, *IS 4031 (Part 6): 1988, Methods of Physical Tests for Hydraulic Cement – Part 6: Determination of Compressive Strength of Hydraulic Cement (Other than Masonry Cement)*, BIS, New Delhi, India.
39 Bureau of Indian Standards, *IS 4031 (Part 8): 1988, Methods of Physical Tests for Hydraulic Cement – Part 8: Determination of Transverse and Compressive Strength of Plastic Mortar Using Prism*, BIS, New Delhi, India.
40 T. G. McKenzie, E. Colombo, Q. Fu, M. Ashokkumar and G. G. Qiao, Sono-RAFT polymerization in aqueous medium, *Angew. Chem., Int. Ed.*, 2017, **56**, 12302–12306, DOI: 10.1002/anie.201706771.
41 P. Kruus and T. J. Patraboy, Initiation of polymetizatlon with ultrasound in methyl methacrylate, *J. Phys. Chem.*, 1985, **89**, 3379–3384, DOI: 10.1021/j100261a044.
42 E. Su, M. Yurtsever and O. Okay, A self-healing and highly stretchable polyelectrolyte hydrogel via cooperative hydrogen bonding as a superabsorbent polymer, *Macromolecules*, 2019, **52**, 3257–3267, DOI: 10.1021/acs.macromol.9b00032.
43 T. Vasudevan, S. Das, A. K. Debnath and A. K. Pandey, Facilitated transport of europium(III) ions across fixed-site membrane, *J. Membr. Sci.*, 2009, **342**, 113–120, DOI: 10.1016/j.memsci.2009.06.03.
44 S. A. Shaikh, K. Rajpurohit, A. K. Pandey and H. K. Bagla, Engineering Portland cement and concrete with agricultural-origin functional additives: Valorization of agro-waste, *Next Sustainability*, 2025, **6**, 100173, DOI: 10.1016/j.nxsust.2025.100173.
45 K. Rajpurohit, S. A. Shaikh, A. K. Pandey and H. K. Bagla, Synthetic polymers and nanostructured materials additives for engineered cementitious materials: Plausible route for recycled polymer utilization, *Hybrid Adv.*, 2025, **11**, 100555, DOI: 10.1016/j.hybadv.2025.100555.
46 S. A. Shaikh, K. Rajpurohit, E. H. M. Malik, A. K. Pandey and H. K. Bagla, Bulk formation of zwitterionic microgel with additives by gamma radiation for large-scale application in self-healing cement, *J. Radioanal. Nucl. Chem.*, 2026, **335**, 1527–1541, DOI: 10.1007/s10967-026-10732-3.